JOURNAL OF APPLIED PHYSICS **113**, 244503 (2013)

Balance between light trapping and charge carrier collection: Electro-photonic optimization of organic photovoltaics with ridge-patterned back electrodes

Yingchi Liu,[1] Cary A. Tippets,[2] Christoph Kirsch,[3] Sorin Mitran,[4] Edward T. Samulski,[5] and Rene Lopez[1,a)]

[1]*Department of Physics and Astronomy, University of North Carolina at Chapel Hill Phillips Hall, CB 3255, Chapel Hill, North Carolina 27599, USA*
[2]*Curriculum in Applied Sciences and Engineering, University of North Carolina at Chapel Hill Phillips Hall, CB 3255, Chapel Hill, North Carolina 27599, USA*
[3]*Institute of Computational Physics, Zurich University of Applied Sciences, Wildbachstrasse 21, 8401 Winterthur, Switzerland*
[4]*Department of Mathematics, University of North Carolina at Chapel Hill Phillips Hall, CB 3250, Chapel Hill, North Carolina 27599, USA*
[5]*Department of Chemistry, University of North Carolina at Chapel Hill Caudill Laboratories, CB 3290, Chapel Hill, North Carolina 27599, USA*

(Received 6 May 2013; accepted 6 June 2013; published online 27 June 2013)

Light trapping strategies are frequently suggested to improve organic photovoltaic (OPV) cell efficiencies. However, one cannot overlook the side-effects to charge carrier collection which are introduced when seeking optical enhancements. A comprehensive electro-photonic model is utilized to study the optical and electrical effects of patterning poly[[4,8-bis[(2-ethylhexyl)oxy]benzo[1,2-b:4,5-b′]dithiophene-2,6-diyl][3-fluoro-2-[(2-ethylhexyl)carbonyl]thieno[3,4-b]thiophenediyl]] and poly(3-hexylthiophene) based solar cells with simple optical grating structures. It is found that for the most part, optical absorption improvements are attenuated by enhanced electrical losses. Optimized device structures that overcome this tradeoff are proposed and their detailed electro-optical characteristics are discussed. When the hole mobility is smaller than the electron mobility, the results suggest that in general, an inverted structure has a better chance to outperform a flat active layer than a conventional architecture in an OPV cell with the ridge-patterned back electrode.
© *2013 AIP Publishing LLC*. [http://dx.doi.org/10.1063/1.4812235]

I. INTRODUCTION

Over the past few years, the field of organic photovoltaics (OPVs) has achieved several critical milestones. The boundary of OPV power conversion efficiencies (PCE) has been continuously elevated to above 9%.[1] OPV could become an important technology in energy landscape in the near future, due to the potential low cost of the polymeric materials and importantly, OPV's amenability to very inexpensive, large area, roll-to-roll manufacturing techniques. Besides developing new photovoltaic materials, favorable device geometrical designs have been studied in order to increase the photo-conversion efficiencies. For instance, the bulk heterojunction (BHJ) morphology, remedied to a large extent the difficulties associated with the intrinsic short exciton (or electron-hole pair) diffusion length (~10 nm), which limits charge separation efficiency.[2,3] In addition to charge separation, the relative short transport length of the separated charges across the convoluted BHJ morphology remains a constraint preventing OPV systems from reaching their full potential, limiting the thickness of the active layer and the total light absorption. Photonic crystal structures have been proposed to counteract charge transport losses by increasing light absorption. The light trapping enhancement of photonic crystal structures has been frequently demonstrated.[4–19] However, it has both advantages and disadvantages: OPV patterned photonic structures not only effectively change a device's optical characteristics but also its electrical performance.[11,18,20] Most device patterning investigations have concentrated on the total optical absorption improvement,[17] while fewer studies focused on investigations of the complete optical and electrical changes due to the patterned structures in organic BHJ solar cells.[11,12,18] Although electro-photonic simulations have been applied to the nanostructured OPV devices,[9,11] detailed discussion of optical and electric consequences from patterning the devices, especially the BHJ layers, has not been presented. Moreover, most of the previous studies were limited to the comparison between devices with normalized parameters (i.e., maintaining the same volume of active material). It is important to also determine the global enhancement by comparison to an optimized flat layer device, though those studies legitimately demonstrated absorption enhancement by the patterned structures.

Our recent work has experimentally demonstrated that realizing a global maximum is not a simple task as electrical deterioration counteracts light absorption gains[18] and there is a strong relationship between the optical absorption profile and bimolecular recombination losses.[21] In this work, we apply a combined electro-photonic model to study both electrical and

[a)]Author to whom correspondence should be addressed. Electronic mail: rln@physics.unc.edu. Tel.: 919-962-7216. Fax: 919-962-0480.

 © 2013 AIP Publishing LLC

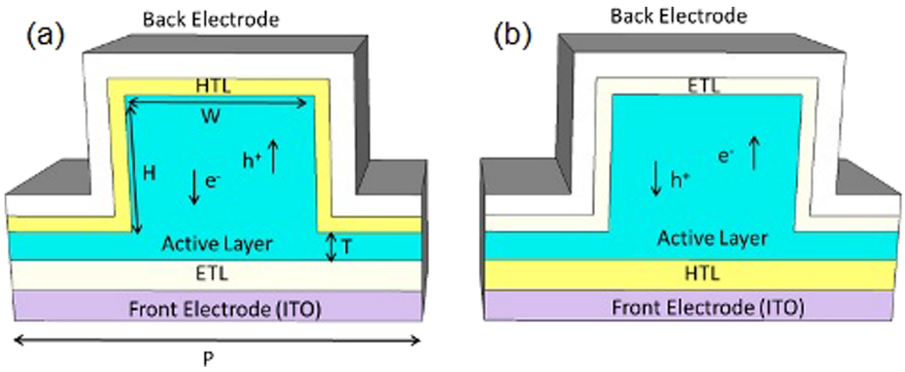

FIG. 1. Sketch of the inverted and conventional grating structures: (a) In an inverted device, electrons are collected in the front electrode after being selected by the electron transport layer (ETL) and holes are collected in the back electrode after being selected by the hole transport layer (HTL) in the inverted device. (b) The opposite charge transport direction defines the conventional structure. Dimensions W, T, H, and P were varied numerically.

optical effects arising from patterning a simple grating structure by comprehensive multiphysics simulations in Poly [[4,8-bis[(2-ethylhexyl)oxy]benzo[1,2-b:4,5-b′]dithiophene-2,6-diyl][3-fluoro-2-[(2-ethylhexyl)carbonyl]thieno[3,4-b] thiophenediyl]] (PTB7) and poly(3-hexylthiophene) (P3HT) devices. It is found that for the most part, optical absorption improvements are indeed limited by enhanced electrical losses. Optimized device structures that overcome this trade-off are proposed and their detailed electro-optical characteristics are discussed. In the case where the hole's mobility is smaller than the electron's, the results suggest that in general an inverted structure has a better chance to outperform the flat architecture than a conventional structure in the OPVs with ridge-patterned back electrode.

II. THEORETICAL APPROACH

A. Materials and structures

PTB7: [6,6]-phenyl C_{71}-butyric acid methyl ester ($PC_{70}BM$) is demonstrated to have > 9% PCE in experiment,[1,22] which is one of the highest efficiencies in the recent literature. In this paper, we focus our discussion on a model for PTB7: $PC_{70}BM$ devices. Additionally, we test the overall conclusions with a distinct set of parameters that represent devices with P3HT: [6,6]-phenyl-C61-butyric acid methyl ester ($PC_{60}BM$) blend, the most widely studied OPV system (see Fig. S1).[32] BHJ devices contain a phase separated blend of an electron donor (PTB7 or P3HT) and electron acceptor ($PC_{70}BM$ or $PC_{60}BM$). Upon photon absorption, an electron-hole pair is created. The phase separation must be close to the electron-hole pair diffusion length in order to generate high free carrier concentrations. The exciton generation profile is therefore approximated as the light absorption profile. Free carriers drift and diffuse through percolation pathways to their respective electrodes for collection.

Here, we studied 2D ridge pattern/gratings in both inverted and conventional BHJ organic solar cell devices with ridge-patterned back electrodes in the OPV material systems (Fig. 1). The devices' electrical properties used in the simulation are listed in Table I and are estimated based on recent literatures and fittings to experimental results.[20,22–24] Optical properties were obtained from our own ellipsometry measurements. In an inverted (Fig. 1(a)) OPV, the device's structure is a stack of indium tin oxide (ITO)/poly [(9,9-bis (3′-(N, N-dimethylamino)propyl)-2,7-fluorene)-alt-2,7-(9,9–dioctylfluorene)] (PFN)/blend/tungsten trioxide(WO_3)/Ag (or Al). The conventional (Fig. 1(b)) structure is ITO/poly (3,4-ethylenedioxythiophene):poly(styrenesulfonate)(PEDOT: PSS)/blend/Ca/Ag(or Al). The choice of electron/hole transport layers (ETL/HTL) and electrodes were studied experimentally.[4,13,18,22,24–26] We simulated both flat and patterned devices for comparison and discussion.

B. Numerical model

For the electrical simulation, we used a mathematical model based on an effective medium approximation of the BHJ material (the ETL/HTL and electrode layers are not explicitly included but their effect is accounted for through boundary conditions enclosing the BHJ).[27] The electric potential ψ [V] in the active material is related to the electron and hole number densities n, p [m^{-3}] by the classical semiconductor equations.[28] These partial differential equations describe charge carrier drift in the electric field, $-\nabla\psi$ [V m^{-1}], as well as diffusion, which yields expressions for the charge carrier fluxes, J_n, J_p [$m^{-2}s^{-1}$] (refer to Eq. (1)). Poisson's equation for electrostatics relates the electric potential ψ to the charge density $-q(n-p)$ [C m^{-3}], where q denotes the elementary charge. The exciton generation rate density in BHJ is computed from an auxiliary optics simulation of the whole device.[29] The exciton generation rate computed by the optics simulation is part of the net charge carrier generation rate which appears as a source term in the charge carrier transport equations. In addition to exciton generation, this source term also incorporates exciton dissociation and decay as well as charge carrier recombination. Here, we neglected exciton diffusion by assuming that the characteristic length scales of both donor and acceptor phases in the bulk heterojunction material are comparable to the

TABLE I. Parameters used for Simulation of PTB7:$PC_{70}BM$ devices.

Electron mobility μ_n (m^2 $V^{-1}s^{-1}$)	5.80×10^{-7}	e/h pair separation distance (m)	1.8×10^{-9}
Hole mobility μ_p (m^2 $V^{-1}s^{-1}$)	1.70×10^{-7}	e/h pair decay rate (s^{-1})	2×10^{-4}
Built in voltage (eV)	1.15	Dielectric constant	3.4

exciton diffusion length. The boundary values of n, p, and ψ are prescribed and depend on the bias voltage. The full details on this approach are reported elsewhere.[20]

III. RESULTS AND DISCUSSION

A. Flat devices

As a benchmark, flat devices were simulated first. PTB7 devices with Ag electrode are used as an example for discussion in the rest of the paper (P3HT-based device results are analogous and can be found in the supplemental information file). Calculated short circuit current density (J_{sc}) and open circuit voltage (V_{oc}) agree well with previously published experimental results.[16,18,22,24–26,30] Fig. 2 shows the J-V curves of the most efficient PTB7/Ag devices for the conventional and inverted flat devices structures, 8.88% and 9.79%, respectively. The slightly higher simulated fill factors (FFs) probably result from ignoring the parasitic resistance of substrates,[11,23] which will not affect our discussion of effects from patterning the active layer. In Fig. 3, the dilemma between the light absorption and free carrier transport is clear in the flat case. The optical absorptions approach a maximum value as the thicknesses increase, while the efficiencies start to drop when the active layer become larger than 200 nm thick.

B. Patterned devices

Figures 2 and 3 also show the J–V (only the best ones) and overall-PCE results for patterned conventional and patterned inverted structures after exploring a wide parameter space. The computer algorithm automatically varied four parameters (i.e., grating period P, ridge height H, width W, and flat layer thickness T) and optimized the structures to find the highest possible efficiencies in both inverted and conventional devices. Along this optimization process, each simulated structure performance was recorded. To have a clear comparison between patterned and flat devices, the PTB7 devices' absorptions and efficiencies are also plotted against the effective thickness of the active layer, which is the average thickness over one period of the grating (Fig. 3). Compared to the optimal flat device, there are many structures that significantly increase the absorption without adding a lot of thickness

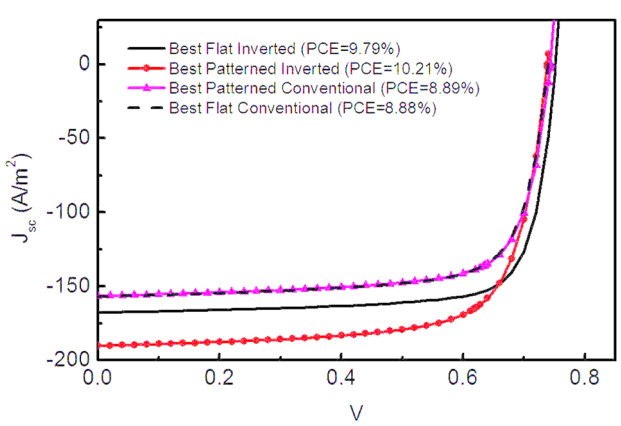

FIG. 2. Simulated current density vs. applied electric potential characteristics for best performing PTB7:$PC_{70}BM$ (flat and patterned) devices.

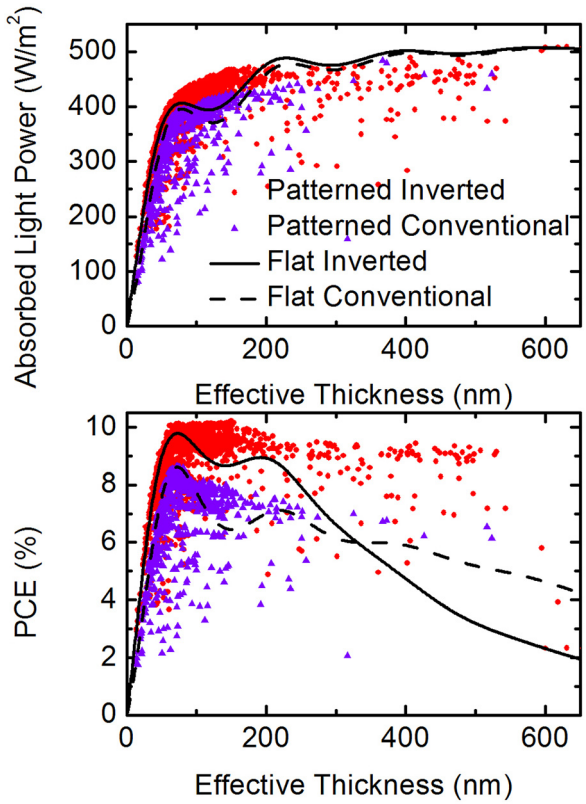

FIG. 3. Absorption vs. effective thickness (a) and PCE vs. effective thickness (b) of both inverted (ITO/PFN/PTB7:$PC_{70}BM/WO_3$/Ag) and conventional (ITO/PEDOT:PSS/PTB7:$PC_{70}BM$/Ca/Ag) devices in the flat and patterned structures.

(See Fig. 3(a)). The absorption enhancement spectra of these devices are comparable to previously published experimental results.[6] However, the PCE can only be improved by a small amount (relative 4%) from 9.79% to 10.21% by grating structures in the inverted case. The PCE enhancement is more trivial in the conventional case. We can see that as efficiency declines with layer thickness in flat devices, many patterned structures are predicted to be able to maintain above 9% PCE at large effective thicknesses. However, an enhancement compared to the most efficient flat layer device is found in much fewer grating structures. This is easier to appreciate in Fig. 4 (output-power/absorbed-power vs. absorbed-power/input-power), where many patterned structures enhance optical absorption (i.e. absorbed power to input power ratio greater than that of the most efficient flat cell). But, nevertheless, the output power to absorbed power ratios is lower than the flat device's value, which means the charge transport is degrading the devices' performance. Hence, the number of patterned devices outperforming the most efficient flat one is actually quite limited.

The overall PCE in the patterned devices does not follow the absorption increase (or decrease), because the grating structures affect the charge carrier collection as well. Choosing inverted PTB7 OPVs (ITO/PFN/PTB7:$PC_{70}BM/WO_3$/Ag) as an example for discussion, let us focus on the effective thickness less than 300 nm where the simulation is crowded with high PCE devices. The computed dissociation probabilities of electron-hole pairs are fairly the same in

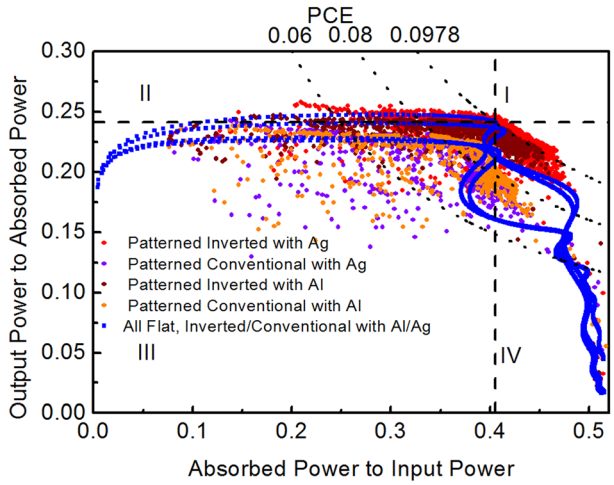

FIG. 4. Efficiency plots: The flat and patterned PTB7 devices' output power to absorbed power vs. absorbed power to input power. The product of these two values is the PCE of one device. Intersection of the dashed lines marks the best flat device. Region I: both electrical and optical enhancements. Region II: Electrical enhancement but optical deterioration. Region III: both electrical and optical deteriorations. Region IV: optical enhancement but electrical deterioration.

patterned and flat devices and hence the electrical effect of patterning can be mainly revealed from carrier collection or transport. Fig. 5 shows that the improvements of light absorption and carrier collection efficiency (number of collected carriers to number of generated carriers, η) do not occur at the same place in most of the cases. Almost all the carrier collections efficiencies of the devices with effective thickness less than 160 nm are deteriorated by patterning, while most of the optical enhancements occur in this range. The carrier collection efficiency is improved by patterning the devices with a large volume but optical enhancement is considerably less. The product of these two ratios is a combination of optical and electrical effects of patterning, which will clearly reflect the possible enhancement in terms of PCE. The maximum of that value locates at the effective thickness of ~140 nm (Fig. S2).[32] It agrees that the largest relative enhancements also occur around 140 nm, where the efficiencies of the flat devices have a local minimum (Fig. 3(b)).

The comparison between patterned and flat devices with the same volume (i.e., effective thickness) does not necessarily lead to an overall optimal configuration. It is important to compare all the patterned devices against the flat one with the highest PCE. In Fig. 6, similarly one can see that the optical enhancements are limited by the electrical deterioration when the patterned devices were compared against the best flat one. This combined effect makes the best pattern device to be the one with p = 410 nm, h = 210 nm, w = 240 nm, t = 80 nm and effective thickness ~150 nm. Although the best patterned device absorbed 14.7% more power than the best flat one, its η value is 89.17%, which is lower than the η (= 93.75%) of the best flat one. The PCE only outperforms the best flat device by ~4% (due to a lower V_{oc} as well). This enhancement is considerably less than the 17.5% improvement when compared with a non-optimized flat device of equal active volume (150 nm thickness).

C. Effect of patterning on internal electric fields and charge collection

It is observed in Figures 3 and 4 that patterning is more beneficial in inverted devices than in conventional configurations. To explore the internal field effects of patterning, we compared inverted (ITO/PFN(10 nm)/PTB7:$PC_{70}BM$/WO_3(15 nm)/Ag) and conventional (ITO/WO_3(15 nm)/PTB7:$PC_{70}BM$/PFN(10 nm)/Ag) structures with each other and with flat structures. The blend in either of these two structures absorbs a similar amount of light (Fig. S3).[32] The difference between the inverted and conventional devices must come from the electrical effects. We simulated 400 nanostructure configurations in which the inverted patterned devices outperform the best flat inverted cell of PTB7: $PC_{60}BM$ in terms of overall PCE. The electron-hole generation profiles and electric field over the cross section of one typical such best structures are plotted in Figs. 7 and in 8, respectively. One can see that in the ridge region there is a weak electric field area, populated with many free carriers. This agrees with previous studies and limits enhancement of PCE by light trapping patterning of OPVs.[11,18] The holes are identified as slower carriers in this type of devices.[22] Due to the weak electric field in

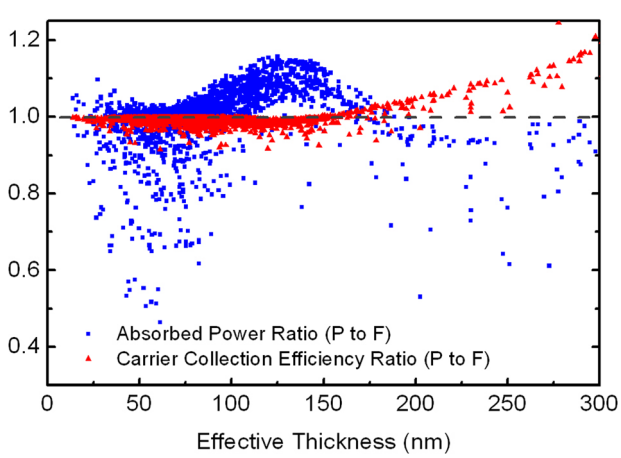

FIG. 5. The ratios of absorbed power of the patterned devices to that of the flat devices with the same volumes (blue) and the ratios of carrier collection efficiency to that of the flat devices with the same volumes (red).

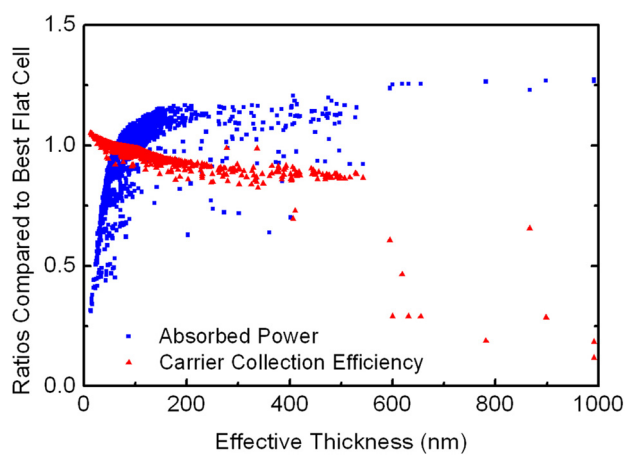

FIG. 6. The ratios of absorbed power of patterned devices to that of the best flat device and the ratios of carrier collection efficiency to that of the best flat device.

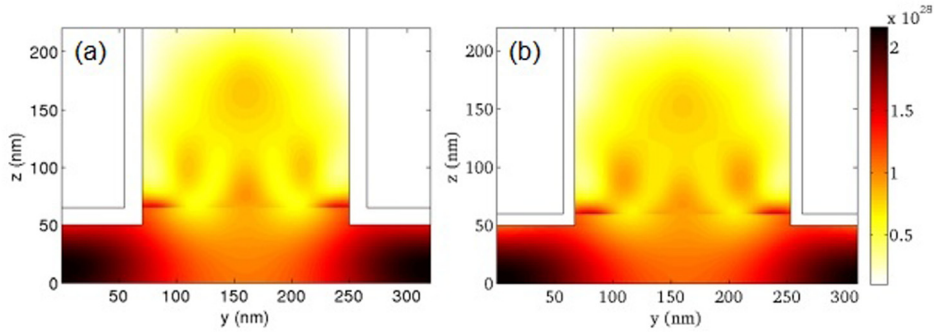

FIG. 7. Electron-hole pair generation rate density ($m^{-3}s^{-1}$) profile of active layers in one inverted device (a) (ITO/PFN/PTB7:PC_{70}BM/WO_3/Ag) and one conventional device (b) (ITO/WO_3/PTB7:PC_{70}BM/PFN/Ag).

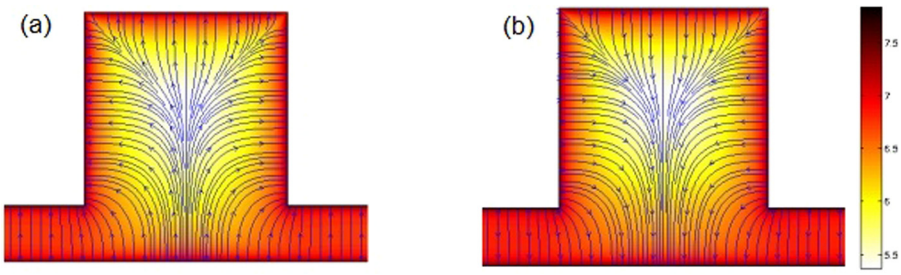

FIG. 8. Log_{10} of the electric field strength ($V\,m^{-1}$) profile of the inverted (a) and conventional (b) devices shown in Fig. 7.

the ridge region, it is closer, and hence easier for holes in that area to be collected by the back electrode (Ag/Al) on the ridge sides in the inverted devices. In conventional devices, on the other hand, the holes need to go to the front electrode, which is relatively farther away. This, we believe, is one possible reason that inverted patterned devices work better than the conventional ones in most cases (Fig. 9(a)).

The pattern also has important effects in the internal charge current densities. The charge carrier flux is a combination of drift and diffusion contributions,

$$J_n = J_{drift} + J_{diffusion} = \mu_n n \nabla\psi - D_n \frac{dn}{dx}, \tag{1a}$$

$$J_p = J_{drift} + J_{diffusion} = -\mu_p p \nabla\psi - D_p \frac{dp}{dx}. \tag{1b}$$

The D_n and D_p are the diffusion coefficients of electron and hole, respectively. We plot electron/hole flux over the cross section (Figs. 10 and S4). It is noted that an observable electron back flow is found at the ridge corners in inverted devices, while the hole back flow is found in the conventional one. The diffusion current is to the opposite direction of drift current and overwhelms the drift current at those corners. The hole current flux in the conventional case is more affected than the electron current flux in the inverted case, which can be related to the slower hole mobility and hence a smaller drift term. This was confirmed by simply running simulations where the electron and hole mobilities are exchanged as input to the numerical program (Fig. S4).[32]

PCE goes down faster in flat inverted devices than in flat conventional devices as thickness increases (Fig. 9(a)) because the slower charge carriers (i.e., holes) are generated farther away from the back electrode, where holes are collected in the inverted devices.[21,31] In contrast, most of the patterned inverted devices have higher efficiencies comparing with their conventional counterparts. And the most efficient

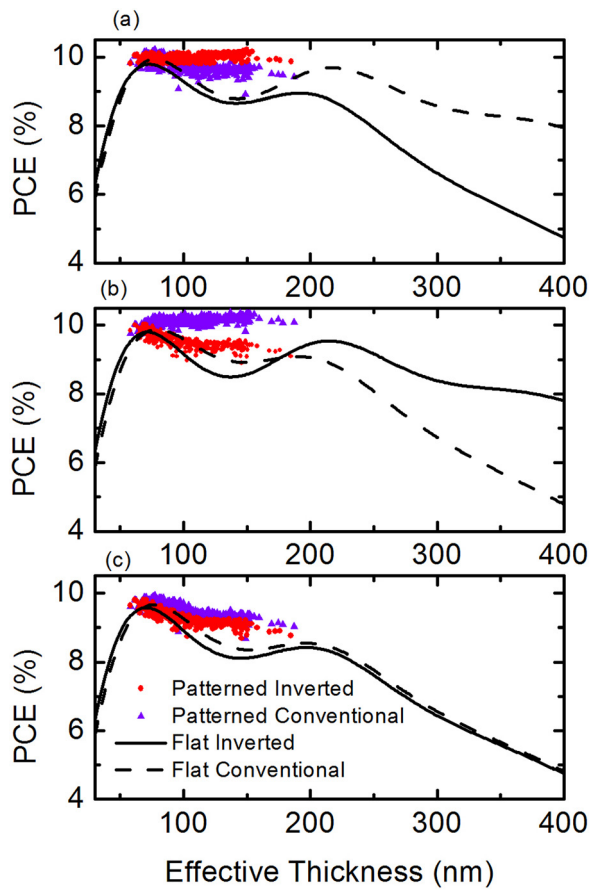

FIG. 9. Simulations of patterned inverted devices (ITO/PFN/PTB7:PC_{70}BM/WO_3/Ag) and conventional devices (ITO/WO_3/PTB7:PC_{70}BM/PFN/Ag). Black Solid and dashed lines are the flat inverted and conventional devices, respectively. Red round dots are the patterned inverted devices and violet triangles dots are the patterned conventional devices. (a) Electron mobility is greater ($\mu_n = 5.8 \times 10^{-7}\,m^2/V\,s$, $\mu_p = 1.7 \times 10^{-7}\,m^2/V\,s$). (b) Hole mobility is greater ($\mu_n = 1.7 \times 10^{-7}\,m^2/V\,s$, $\mu_p = 5.8 \times 10^{-7}\,m^2/V\,s$). (c) Electron and hole mobilities are equal ($\mu_n = 1.7 \times 10^{-7}\,m^2/V\,s$, $\mu_p = 1.7 \times 10^{-7}\,m^2/V\,s$).

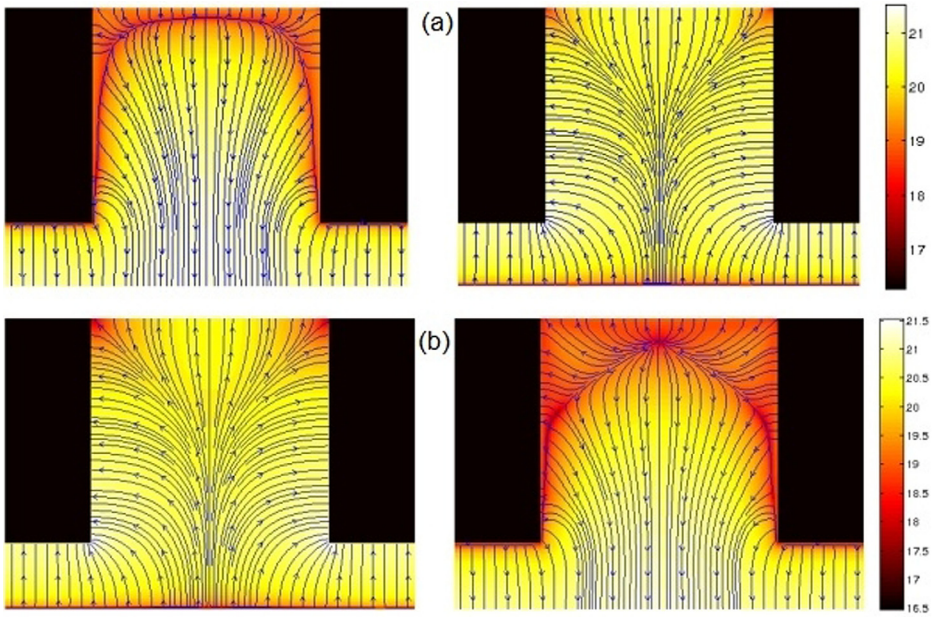

FIG. 10. Electron (left) and hole (right) flux ($m^{-2}s^{-1}$) (a) inverted devices (b) conventional devices when electron mobility is greater than the hole mobility ($\mu_n = 5.8 \times 10^{-7}\,m^2/V\,s$, $\mu_p = 1.7 \times 10^{-7}\,m^2/V\,s$).

device has an inverted structure. However, if the input hole and electron mobilities are exchanged, the simulation results will be the opposite (Fig. 9(b)). And there is no significant difference between the choice of conventional and inverted structures, if the electron and hole have equal mobilities (Fig. 9(c)). Furthermore, the differences between patterned inverted and conventional devices' efficiencies are larger in the case of greater difference between electron and hole mobilities (Fig. S5).[32] These interesting results suggest that when patterning an OPV the mobilities must be considered to determine the optimal structure (inverted or conventional) for the material. One should apply the inverted structure to improve preserve carrier collection when patterning OPVs, if the hole is tested to be the slower carrier.

IV. CONCLUSIONS

By an electro-photonic model, we have simulated the performance of flat and patterned grating electrodes in OPV devices. Optimized 2D grating structures for the active layer patterning are proposed. Additionally, we discussed the trade-off between light trapping enhancement and charge carrier transport deterioration induced by those structures. The grating structure may not only weaken the local electric field but also may change the generation profile inside the active layer and hence affect the distance of the free carriers from the electrodes. These effects demonstrate that mere light absorption improvement by patterning devices is not sufficient. The total enhancement is a combination of all electrical and optical effects. Moreover, our results provide guidance on the choice of polarity of electron/hole current flows in inverted or conventional device structures. We found that there is a greater chance to improve devices' efficiencies in the patterned inverted structures when the hole transport is slower.

ACKNOWLEDGMENTS

Support for this work from NSF (Solar:DMR-0934433) is gratefully acknowledged.

[1]Z. He, C. Zhong, S. Su, M. Xu, H. Wu, and Y. Cao, Nature Photon. **6**, 591 (2012).
[2]J. J. M. Halls, C. A. Walsh, N. C. Greenham, E. A. Marseglia, R. H. Friend, S. C. Moratti, and A. B. Holmes, Nature **376**, 498 (1995).
[3]G. Yu, J. Gao, J. C. Hummelen, F. Wudl, and A. J. Heeger, Science **270**, 1789 (1995).
[4]X. H. Li, W. E. I. Sha, W. C. H. Choy, D. D. S. Fung, and F. X. Xie, J. Phys. Chem. C **116**, 7200 (2012).
[5]P. Wang and R. Menon, Opt. Express **21**, 6274 (2013).
[6]J. You, X. Li, F. Xie, W. E. I. Sha, J. H. W. Kwong, G. Li, W. C. H. Choy, and Y. Yang, Adv. Energy Mater. **2**, 1203 (2012).
[7]S. Mokkapati and K. R. Catchpole, J. Appl. Phys. **112**, 101101 (2012).
[8]D. H. Wang, J. Seifter, J. H. Park, D.-G. Choi, and A. J. Heeger, Adv. Energy Mater. **2**, 1319 (2012).
[9]W. E. I. Sha, W. C. H. Choy, Y. Wu, and W. C. Chew, Opt. Express **20**, 2572 (2012).
[10]S.-I. Na, S.-S. Kim, J. Jo, S.-H. Oh, J. Kim, and D.-Y. Kim, Adv. Funct. Mater. **18**, 3956 (2008).
[11]W. Vervisch, G. Rivière, S. Vedraine, S. Biondo, P. Torchio, D. Duché, J.-J. Simon, and L. Escoubas, J. Appl. Phys. **111**, 094506 (2012).
[12]V. K. Narasimhan and Y. Cui, Nanophoton. **0**, 1 (2013).
[13]X. Li, W. C. H. Choy, L. Huo, F. Xie, W. E. I. Sha, B. Ding, X. Guo, Y. Li, J. Hou, J. You, and Y. Yang, Adv. Mater. **24**, 3046 (2012).
[14]D.-H. Ko, J. R. Tumbleston, L. Zhang, S. Williams, J. M. DeSimone, R. Lopez, and E. T. Samulski, Nano Lett. **9**, 2742 (2009).
[15]D.-H. Ko, J. R. Tumbleston, A. Gadisa, M. Aryal, Y. Liu, R. Lopez, and E. T. Samulski, J. Mater. Chem. **21**, 16293 (2011).
[16]K. S. Nalwa, J.-M. Park, K.-M. Ho, and S. Chaudhary, Adv. Mater. **23**, 112 (2011).
[17]L. Chen, W. E. I. Sha, and W. C. H. Choy, Opt. Express **20**, 8175 (2012).
[18]Y. Liu, C. Kirsch, A. Gadisa, M. Aryal, S. Mitran, E. T. Samulski, and R. Lopez, J. Phys. D: Appl. Phys. **46**, 024008 (2013).
[19]X. Li, W. C. H. Choy, H. Lu, W. E. I. Sha, and A. H. P. Ho, Adv. Funct. Mater. **23**, 2728 (2013).
[20]C. Kirsch and S. Mitran, J. Appl. Phys. **112**, 054502 (2012).
[21]J. R. Tumbleston, Y. Liu, E. T. Samulski, and R. Lopez, Adv. Energy Mater. **2**, 477 (2012).
[22]Y. Liang, Z. Xu, J. Xia, S.-T. Tsai, Y. Wu, G. Li, C. Ray, and L. Yu, Adv. Mater. **22**, E135 (2010).
[23]J. R. Tumbleston, D.-H. Ko, E. T. Samulski, and R. Lopez, J. Appl. Phys. **108**, 084514 (2010).
[24]Z. He, C. Zhong, X. Huang, W.-Y. Wong, H. Wu, L. Chen, S. Su, and Y. Cao, Adv. Mater. **23**, 4636 (2011).
[25]A. Gadisa, Y. Liu, E. T. Samulski, and R. Lopez, ACS Appl. Mater. Interfaces **4**, 3846 (2012).
[26]C. Tao, S. Ruan, G. Xie, X. Kong, L. Shen, F. Meng, C. Liu, X. Zhang, W. Dong, and W. Chen, Appl. Phys. Lett. **94**, 043311 (2009).

[27]L. J. A. Koster, E. C. P. Smits, V. D. Mihailetchi, and P. W. M. Blom, Phys. Rev. B **72**, 085205 (2005).
[28]W. van Roosbroeck, Bell Syst. Tech. J. **29**, 560 (1950).
[29]S. G. Tikhodeev, A. L. Yablonskii, E. A. Muljarov, N. A. Gippius, and T. Ishihara, Phys. Rev. B **66**, 045102 (2002).
[30]M. T. Dang, L. Hirsch, and G. Wantz, Adv. Mater. **23**, 3597 (2011).
[31]J. R. Tumbleston, D.-H. Ko, E. T. Samulski, and R. Lopez, Phys. Rev. B **82**, 205325 (2010).
[32]See supplementary material at http://dx.doi.org/10.1063/1.4812235 for supplemental figures.

View publication stats